行政院國家科學委員會專題研究計畫 成果報告

植栽圍籬對住宅建築周圍氣流影響之研究
研究成果報告(精簡版)

計 畫 類 別 ：個別型
計 畫 編 號 ：NSC 95-2415-H-216-002-
執 行 期 間 ：95 年 08 月 01 日至 96 年 07 月 31 日
執 行 單 位 ：中華大學景觀建築學系

計 畫 主 持 人：張瑋如

計畫參與人員： 大學生-兼任助理：吳欣樺、黃建傑、李典桂

處 理 方 式 ：本計畫可公開查詢

中 華 民 國 96 年 10 月 08 日

附件一

行政院國家科學委員會補助專題研究計畫 ■ 成 果 報 告 □期中進度報告

（計畫名稱）

植栽圍籬對住宅建築周圍氣流影響之研究

計畫類別：■ 個別型計畫　　□ 整合型計畫
計畫編號：NSC 95-2415-H-216-002
執行期間：95 年 08 月 01 日至 96 年 07 月 31 日

計畫主持人：張瑋如
共同主持人：
計畫參與人員： 吳欣樺、黃建傑、李典桂

成果報告類型(依經費核定清單規定繳交)：■精簡報告　□完整報告

本成果報告包括以下應繳交之附件：
□赴國外出差或研習心得報告一份
□赴大陸地區出差或研習心得報告一份
□出席國際學術會議心得報告及發表之論文各一份
□國際合作研究計畫國外研究報告書一份

處理方式：除產學合作研究計畫、提升產業技術及人才培育研究計畫、列管計畫及下列情形者外，得立即公開查詢
□涉及專利或其他智慧財產權，□一年□二年後可公開查詢

執行單位：中華大學

中　華　民　國　96 年　10 月　10 日

ABSTRACT

The present paper has performed a three-dimensional numerical model to study the cross ventilation in a residential building. Examined are the effects of porous hedge placed ahead of the building, and focused are the physical procedures governing air movement during the cross ventilation. The ratio of the space between the hedge and the building to the hedge height is fixed at L/h=2.0, while the hedge porosity is varied from η=0 to 1.0. Detailed information about the mean velocity, pressure, and turbulent kinetic energy is provided to illustrate how the porous hedge affects the cross ventilation in a building of two-side openings. It is found that the porous hedge could modify the mean and turbulent flow structures behind it, and thus alter the cross ventilation of the building. Three types of cross ventilation can be characterized from the results presented, i.e., backward cross ventilation, null ventilation, and forward cross ventilation, respectively. Results further show that the distribution of volume-averaged turbulent kinetic energy has a local minimum value at about the null ventilation conditions.

Keywords: Passive control, Porous hedge, Cross ventilation, Porosity

1. Introduction

In a naturally ventilated building, the indoor air is renewed with the outdoor air using wind and/or buoyancy forces. The passive scheme not only improves indoor air quality and thermal comfort [1, 2] but also, when applied properly, leads to a significant reduction of energy consumption in ventilating the buildings [3]. Most importantly, it can avoid the Sick Building Syndrome caused by poor design of active ventilation systems. The combination of the above merits establishes the natural ventilation as the best solution for improving the microenvironment. Consequently, the study of natural ventilation has gained more and more attention in recent years [1-6].

In a typical cross-ventilated building, wind-pressure differences along the facade create a natural air exchange between indoor and outdoor spaces. The ventilation rate depends on the strength and direction of wind forces and the resistance of the airflow path. Direct introduction of outdoor air by wind forces, however, does not necessarily ensure a comfortable indoor environment because it gives no control over undesirable airflow patterns. If the cross ventilation of a building is poorly designed, even with an plenty of wind resources, the period during which windows can be left open is often limited due to uncomfortable wind intrusion. To control wind-driven airflow patterns and thus improving the indoor microclimate, a passive scheme using windbreaks such as forests, nets, and hedges has been employed to modify the cross-ventilation in a building [7]. The porous hedges act not only a shelter from a strong wind but also a regulator to channel airflow properly to ventilate a building. The objective of the present work is to extend the author's 2-D work [7] to develop a 3-D numerical model to study the cross ventilation in a building that are controlled passively by using a porous hedge.

A successful design of wind-driven cross ventilation requires the detailed information of airflow and pressure distributions in and around buildings. The physical processes of wind-driven cross ventilation are complex, and predicting the ventilation rates is difficult. Although full-scale measurements for a building site can provide reliable data, the experiment is time consuming and hard to control. In addition, the discrete data are not informative enough. In most cases, the experimental data obtained from one building site may not be extended to another because of different weather data and building surroundings [5]. An alternative approach to study the cross ventilation in buildings is the computational fluid dynamics (CFD) technique. The CFD technique is becoming popular due to its informative results and low labor and equipment costs. In the present study three-dimensional CFD model is developed to study the cross ventilation in a building that are controlled passively by using a porous hedge. The effect of the hedge porosity on the airflow characteristics in and around a residential building is examined. The phenomena of cross ventilation in the building are discussed from the detailed distributions of mean fluid flow, turbulent kinetic energy, and pressure distributions. The computational procedure, adopted for the evaluation of such a three-dimensional turbulent flow, is based on the solution of the governing equations for the dependent variables (such as three velocity components, the pressure and the turbulent kinetic energy) by means of the finite volume technique [8, 9]. The airflow is assumed to be steady and turbulent, which is described through the well-known k-ε turbulence model. It has been proven to be able to simulate quite well the mean flow and turbulent kinetic energy of a long, porous hedge standing on flat ground [10-12]. In addition, the k-ε model has an advantage of saving computing time, and thus has become the most widely used CFD method in many industrial applications. This is the reason why the model is employed in the present paper in resolving the problem mentioned above.

2. The Model

A schematic drawing illustrating the airflow around a residential building along with a porous hedge is shown in Fig. 1. The origin of the coordinate system is set at the rear edge of the porous hedge. The airflow is from left to right. The porous hedge of height h is placed ahead of the building. The distance between the front edge of the building and the rear edge of the porous hedge is 2h (L). The dimensions of the interior space of the building are 2h by 3h by h (length by width by height). The windward and leeward walls have a window of size 0.5h by h. Both windows are open that allows of cross ventilation in the building.

2.1 Governing equations

The airflow studied is considered as three-dimensional, steady, isothermal, incompressible and turbulent. The fundamental equations governing the motion of the above flow are the averaged Navier-Stokes equations, and the continuity equation, which can be expressed as:

$$\frac{\partial U_i}{\partial x_i} = 0 \tag{1}$$

$$\frac{\partial}{\partial x_i}\left(U_i U_j\right) = -\frac{1}{\rho}\frac{\partial p}{\partial x_i} + \frac{\partial}{\partial x_i}\left(2\nu S_{ij} - \overline{u_i u_j}\right) \tag{2}$$

$$S_{ij} = \frac{1}{2}\left(\frac{\partial U_i}{\partial x_j} + \frac{\partial U_j}{\partial x_i}\right) \tag{3}$$

The turbulent fluxes of momentum ($\overline{u_i u_j}$) are important terms that govern the turbulent diffusion and need to be specified by certain turbulence models in order to fulfill the closure of the equation set. A number of turbulence models, ranging from simple algebraic models to second-moment closure models, have been developed in the past decades. For simplicity, the standard k-ε model is used in closing the equation set. The correlation between the mean turbulent kinetic energy k and the dissipation rate of turbulence ε is expressed by the following equations:

$$\nu_t = \frac{C_\mu k^2}{\varepsilon} \tag{4}$$

$$\overline{u_i u_j} = -2\nu_t S_{ij} + \frac{2}{3}k\delta_{ij} \tag{5}$$

where ν_t is the turbulent diffusivity, and δ_{ij} the Kronecker symbol. The transport equations for k and ε are

$$\frac{\partial}{\partial x_j}\left(U_j k\right) = \frac{\partial}{\partial x_j}\left[\left(\nu + \frac{\nu_t}{\sigma_k}\right)\frac{\partial k}{\partial x_j}\right] + 2\nu_t S_{ij}\frac{\partial U_i}{\partial x_j} - \varepsilon \tag{6}$$

$$\frac{\partial}{\partial x_j}\left(U_j \varepsilon\right) = \frac{\partial}{\partial x_j}\left[\left(\nu + \frac{\nu_t}{\sigma_k}\right)\frac{\partial \varepsilon}{\partial x_j}\right] + 2C_{\varepsilon 1}\nu_t S_{ij}\frac{\varepsilon}{k}\frac{\partial U_i}{\partial x_j} - C_{\varepsilon 2}\frac{\varepsilon^2}{k} \tag{7}$$

The model constants are also the standard values for wind-tunnel flows:

$C_\mu = 0.09$, $C_{\varepsilon 1} = 1.44$, $C_{\varepsilon 2} = 1.92$, $\sigma_k = 1.0$, and $\sigma_\varepsilon = 1.3$ [13]

The flow momentum within the porous hedge is described by the Darcy's law, i.e.,

$$\frac{\partial}{\partial x_i}\left(\eta U_i U_j\right) = -\frac{\eta}{\rho}\frac{\partial p}{\partial x_i} + \frac{\partial}{\partial x_i}\left(2\eta\nu S_{ij}\right) - \frac{\eta^2\nu}{\kappa}U_i \tag{8}$$

where η is the porosity of the hedge, representing the volume occupied by the pores, to the total volume of the porous solid. The permeability κ is a quantity of the surface area to volume ratio of the porous matrix. The last term in the above equation represents the Darcy's drag imposed by the pore walls on the fluid within the pores, and usually results in a significant pressure drop across the porous solid.

2.2 Grid creation and boundary conditions

As shown in Fig. 2, a half-sphere computational domain is employed to simulate the fluid flow characteristics around the hedge and building. In general, the fluid flow around the building and the porous hedge is changed significantly. Therefore, a fine mesh of high spatial resolution is created around these regions so that an accuracy prediction may be obtained. A total of 1,376,900 unstructured control cells are generated from the whole computational domain. Additional runs for a coarser mesh (1,590,000 cells) and a finer mesh (1,000,000 cells) are obtained by checking grid independence. A comparison of the results of the 1,376,900-cell mesh and the 1,590,000-cell mesh shows that the maximum discrepancy in the mean velocity profiles is 0.05 percent. This change is so small that the accuracy of the solutions on a 1,376,900-cell mesh is already satisfactory.

At the inlet of the computational domain (the upstream quarter sphere), a uniform velocity is imposed. At the downstream section (the downstream quarter sphere), the averaged pressure is chosen as the reference pressure. There is no standard method for setting the turbulence kinetic energy and the dissipation rate in the free stream. In the present simulation, we assume a 0.5% turbulence intensity in the free stream. Thus, k and ε at the inlet section can be calculated. All solid boundaries, such as ground and building walls, we use non-slip conditions in conjunction with the wall functions.

2.3. The solution method

In the simulation processes, the highly coupled, nonlinear, partial differential equations are discretized into a set of linear algebraic equations by using the finite volume discretization method. Then, they are solved by iterative solutions on each control cell, defined over the computational domain. A balance between source terms, convention and momentum fluxes is evaluated by the continuity equation at the faces of each cell. The estimation of diffusion fluxes at the cell faces is obtained by a centered approximation, while the first order upwind approximation is adopted for the advection terms. The pressure-velocity linkage is solved via the SIMPLER algorithm [14]. All computations are preceded by using a general-purpose commercial code, in which the above mathematical models have been installed.

3. Results and Discussion

3.1 Verification of the model

Before the subsequent discussion about the computational results, it is important to

validate present numerical procedure and data by comparing the present results with those in previous works. Figure 3 shows a comparison of mean velocity ratios in x (U/U_h) and z (W/U_h) directions between the present predictions and the previous experiments [12]. In this plot, the hedge porosity is fixed at η=0.7, and the axial station selected for comparison is at h/2 behind the hedge. It is seen that both the experimental and simulated results reveal a forward velocity behind the hedge, meaning that there is no flow recirculation. Moreover, both results show a rather uniform distribution of U/U_h for 0.1<z/h<0.9, where the maximum discrepancy is less than 10%. In the previous experiments, however, a large variation of U/U_h and W/U_h occurs at the elevation 0.9<z/h<1.0, where turbulence is significant due to the strong shear flow. In general, the above comparisons are satisfactory to confirm that the present numerical procedure is adequate and the present numerical results reliable.

3.2 Detailed fluid flow

A comparison of mean-flow patterns around the building between the hedge-free case and the solid-hedge case is shown in Figs. 4 and 5. Figure 4 distributes the mean-velocity vectors on the planes cutting across the middle of the computational module (y=0), whereas Fig. 5 visualizes the mean-flow traces around the building. Figures 4 (a) and 5 (a) are the hedge-free cases, while Fig. 4 (b) and 5 (b) are the results that the solid-hedge is placed ahead of the building. The above results serve as a reference to examine the effect of porous hedge on the cross ventilation in the building.

It is seen from Fig. 4 (a) that the hedge-free case has a forward airflow that ventilates the building as it traverses through a sudden contracting and expanding channel. When a solid hedge stands ahead of the building (Fig. 4 (b)), the airflow is deflected significantly when it approaches the solid hedge, and then separates from the upstream salient of the solid hedge. The relatively low pressure behind the solid hedge (will be shown later) induces the airflow upstream. It thus forms a flow recirculation behind the solid hedge that ventilates the building reversely, with a backward airflow from the leeward window to the windward window.

A particle trace is helpful in visualizing the mean-flow structures in a flow domain. It represents well the trajectory of a massless particle moving in a fluid. In Fig. 5, four particles are released at points of (x, y, z) = (6, 0, 2.75), (-1, 0, 2.75), (-1, 4, 1.5), and (-1, -4, 1.5), respectively, and then move through the flow domain. Each trace is shown by a curve together with the velocity vectors. The color mapping is also provided to illustrate the velocity magnitude along the trace. It is seen from these figures that the trace #1 of the hedge-free case penetrates the building directly from the windward window to the leeward window. In contrast, the trace #1 of the solid-hedge case circulates the particle round the building. It enters the building from the leeward window, then exits from the building via the windward window, and finally turns upward and moves downstream over the building roof. Traces #3 and 4 of the hedge-free case impinge on the front wall of the building directly, while those of the solid-hedge case are deflected by the solid hedge and pass the building laterally.

As the discussion of Figs. 4 and 5, the flow structure around the building is strongly affected by the solid hedge. Therefore, before discussing the effect of porous hedge on the ventilated airflow in the building, it is important to understand the mean velocity distribution ahead of the building, which is regarded as the inlet/outlet conditions of the ventilated building. Figure 6 shows the effect of the hedge porosity on the axial velocity (U) at the mid-station (x/h=1.0) between the porous hedge and the building on the symmetric plane of the computational module (y=0). It is seen that due to the blockage effect, the axial velocity decreases with decreasing the hedge porosity from η =1.0 to 0.4. At η = 0.2, a part of airflow moves upstream indicating that a flow reversal exits behind the porous hedge, which is like that of solid hedge (η = 0).

Focus is now put on the effect of porous hedge on the cross ventilation in the building.

Figure 7 compares the distributions of mean-velocity vectors on the plane cutting across the middle of the computational module (y=0) of various hedge porosities, i.e., η = 0.2, 0.4, 0.6 and 0.8. The corresponding pressure distributions on the plane are also provided in Fig. 8. Obviously, the cross ventilation resulting from these four porosities are quite different. At the highest porosity of η = 0.8 (Figs. 7 (a) and 8(a)), the high pressures near the windward window results in a strong airflow into the building. It traverses directly through the building like that of the hedge-free case (Fig. 4 (a)). When the porosity decreases to η =0.6 (Fig. 7 (b)), the strength of forward ventilated airflow is reduced due to a higher blockage of the porous hedge (Fig. 6). Meanwhile, the pressure difference between two windows is lessened (Fig. 8 (b)). As the hedge porosity further decreases to η =0.4 (Fig. 7 (c)), clearly, the indoor airflow is stagnant almost and the indoor pressures are rather uniform (Fig. 8 (c)). At the lowest hedge porosity of η = 0.2 (Fig. 7(d)), the backward airflow ventilates the building from the leeward window to the windward windows by the adverse pressure gradient in the building (Fig. 8(d)). It is similar to that of the solid hedge, which is dominated by the flow recirculation (Fig. 5 (b)) behind the solid hedge [15].

Figure 9 further shows the effect of the hedge porosity on the pressure distribution along the elevation of z/h=0.58 on the symmetric plane of the computational module (y=0). The solid and dashed curves represents the results of the solid-hedge (η = 0) and hedge-free (η = 1.0) cases, respectively. It is observed that the pressure for the hedge-free case (dashed curve) increases before encountering the building due to the blockage effect, decreases to a local minimum in the building, then bumps up and down, and finally recovers, after the lowest point, to normal level. It is further seen that the pressure for the solid-hedge case (solid curve) drops significantly as the airflow across the solid hedge. A relatively low pressure occurs in the region between the solid hedge and the building, which is attributed to the flow reversal. When the porous hedge is placed ahead of the building, the pressures around the hedge and the building are ranged between the solid-hedge case and the hedge-free case. It is interesting to note that the pressures inside the building for η = 0.4 (dotted line) are rather uniform, meaning that the driving force for the cross ventilation is missing. This confirms the results displayed in Fig. 7 (c) showing a stagnant air inside the build.

It is concluded from the above discussion that the cross ventilation inside the building is strongly affected by the hedge porosity. The ventilation in the building can be characterized by thee categories, i.e., the backward cross ventilation (η = 0.2), null ventilation (η ~0.4), and the forward cross ventilation (η = 0.6, and 0.8), respectively.

3.3 Ventilated airflow rate

Figure 10 shows the effect of porous hedge on the ventilated airflow rate through the building. The abscissa of the plot is the hedge porosity, and the ordinate is the airflow rate ratio between the porous-hedge case and the hedge-free case, i.e.,

$$Se = \frac{\left(\int_A \rho \mathrm{U} \mathrm{d}A\right)_{\text{with hedge}}}{\left(\int_A \rho \mathrm{U} \mathrm{d}A\right)_{\text{hedge-free}}} \tag{9}$$

The magnitude of the ventilated airflow rate ratio can represent the shelter effect by the porous hedge. The smaller the absolute value of Se is, the higher the shelter effect of the porous hedge becomes. It is seen from Fig. 10 that the ventilated airflow rate ratio becomes negative as the porosity is lower than 0.37. It indicates adverse ventilation from the leeward window to the windward window. After η>0.37, the ventilated airflow rate ratio increases with increasing the hedge porosity. It can be illustrated by the velocity vectors shown in Fig. 7 and the pressure distributions shown in Fig. 8. Therefore, it is concluded that a critical hedge

porosity at about η = 0.37 which results in null ventilation in the building. It is interested to note that the present critical hedge porosity is higher than that obtained for the previous study [7]. This may be attributed to the present 3-D results accounted for the lateral-flow effect that did not consider in the previous 2-D work. Figure 11 further shows the effect of the hedge porosity on the volume-averaged turbulent kinetic energy in the building. The volume-averaged kinetic energy is represented as the following form,

$$\bar{k} = \frac{\int_{\text{vol.}} k \mathrm{d}v}{6\mathrm{h}^3} \tag{10}$$

It is seen that the value of $\bar{k}$ is high for the both the strong forward ventilation and adverse ventilation. A valley of the curve is found around the null ventilation.

4. Concluding remarks

A three-dimensional numerical model has been performed to examine the effect of porous hedge on the cross ventilation in a residential building. The porosity of the porous hedge is varied from η=0 to 1.0. Results reveal that placing a porous hedge ahead of the building is an effective scheme to modify the cross ventilation by altering the airflow patterns. The cross ventilation inside the building is strongly dependent of hedge porosity. The shelter effect of the porous hedge can be enhanced by decreasing the hedge porosity. An inverse cross-ventilation of the building can be found for low hedge porosity. From the results presented, it can be characterized as the backward cross ventilation for η < 0.37, null ventilation for η ~ 0.37, and the forward cross ventilation for η > 0.37, respectively. Results further show that the distribution of volume-averaged turbulent kinetic energy has a local minimum value at about the null ventilation conditions.

5. References

1. Hunt, G.R., Linden, P.F., The fluid mechanics of natural ventilation-displacement ventilation by buoyancy-driven flows assisted by wind, Building and Environment 1999; 34: 707-720.
2. Aynsley R. Estimating summer wind driven natural ventilation potential for indoor thermal comfort. Journal of Wind Engineering and Industrial Aerodynamics 1999;83:515–25.
3. Eftekhari MM, D'Ovidio. A winter and summer thermal comfort and airflow measurements in a naturally ventilated room Proceedings of the CIBSE A: Building Services Engineering Research & Technology 1999; 20(3): 155–60.
4. Lu, W.Z., Lo, S.M., Fang, Z., Yuen, K.K., A preliminary investigation of airflow field in designated refuge floor, Building and Environment 2001; 36: 219-230.
5. Li, Y., Delsante, A., Natural ventilation induced by combined wind and thermal forces, Building and Environment 2001; 36: 59-71.
6. Chen, Z.D., Li, Y., Buoyancy-driven displacement natural ventilation in a single-zone building with three-level openings, Building and Environment 2002; 37: 295-303.
7. Chang, W.R., Effect of porous hedge on the cross ventilation in a residential building, Building and Environment, 2006; 41: 549-556.
8. Hwang, J.J., Lai, D.Y., Three-dimensional mixed convection in a rotating multiple-pass square channel, International Journal of Heat and Mass Transfer, 1998; 41: 979-991.
9. Hwang, J.J., Chen, C.K., Savinell, R.F., Liu, C.C., Wainright, J., A three-dimensional numerical simulation of the transport phenomena in the cathodic side of a PEMFC, Journal of Applied Electrochemistry, 2004; 34: 217-224.

10. Packwood, A.R., Flow through porous fences in thick boundary layer: comparisons between laboratory and numerical experiments, Journal of Wind Engineering and Industrial Aerodynamics 2000; 88: 1-24.
11. Wilson, J.D., Numerical studies of flow through a windbreak, Journal of Wind Engineering and Industrial Aerodynamics 1985; 21: 119-154.
12. Boldesa, U., Colmana, J., Maranon Di Leo, J., About the penetration of a horizontal axis cylindrical vortex into the nearby downwind region of a vertical porous fence, Journal of Wind Engineering and Industrial Aerodynamics 2003; 91: 859-872.
13. Launder, B.E., Spalding, D.B., The numerical computation of turbulent flow, Computer Methods in Applied Mechanics and Engineering 1974; 3: 269-289.
14. Patankar, S.V., Numerical Heat Transfer and Fluid Flow 1980, Hemisphere, Washington, DC.
15. J.J. Hwang, Turbulent heat transfer and fluid flow in a porous-baffled channel, Journal of Thermophysics and Heat Transfer, 1997; 11: 429-436.

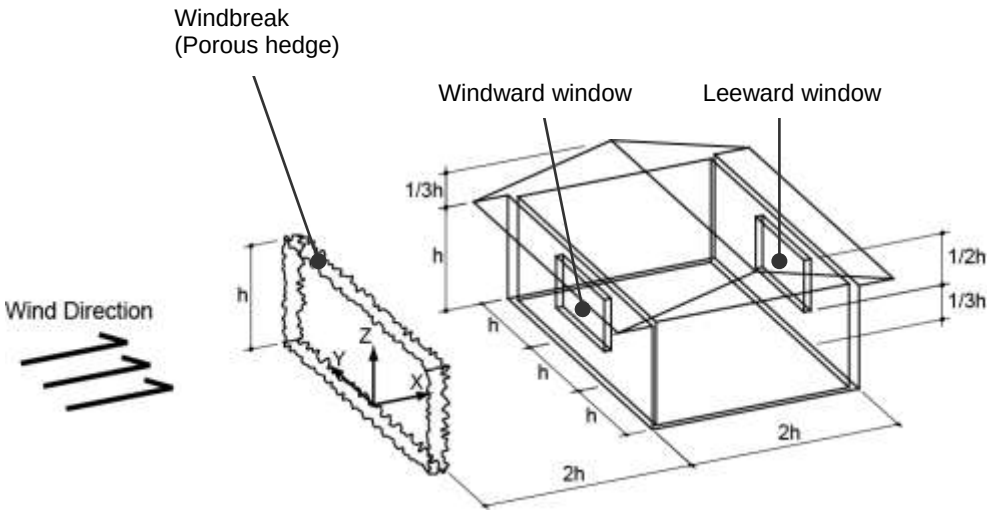

Figure 1 Schematic drawing of the wind-driven cross ventilation around the building.

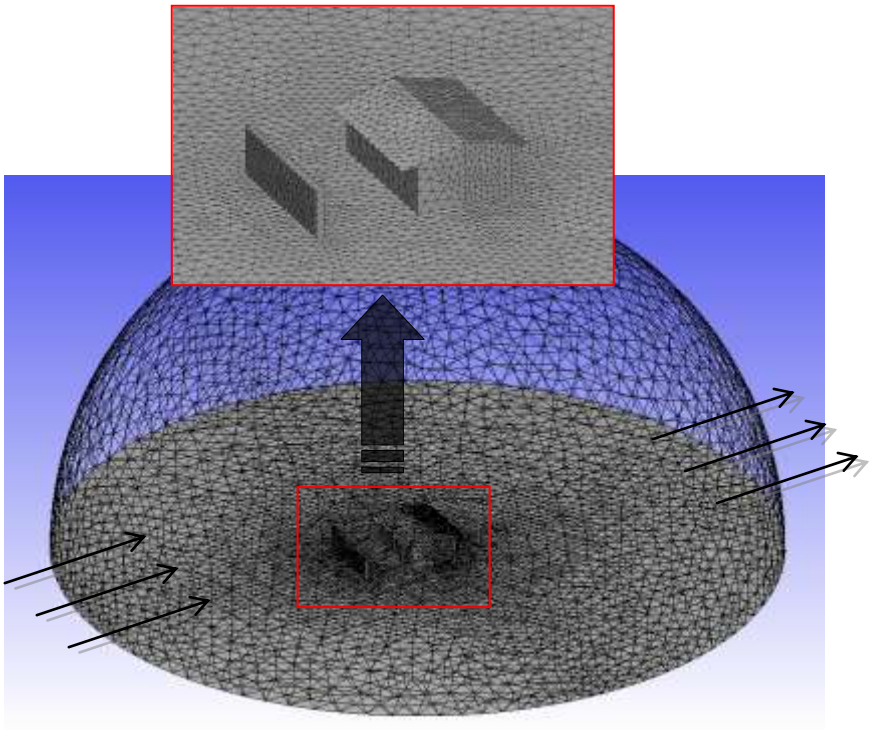

Figure 2 Mesh distributions on the computational domain.

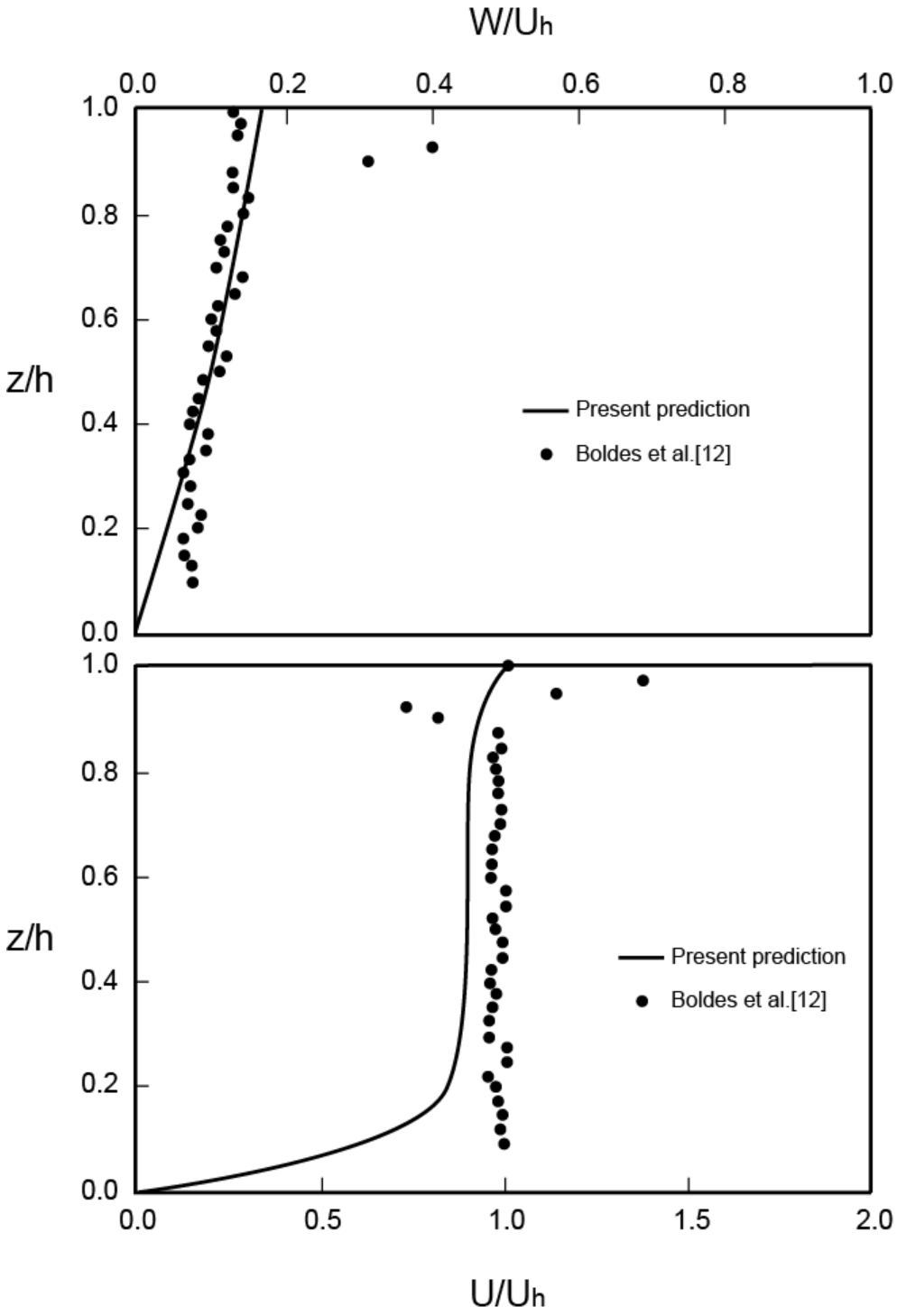

Figure 3 Comparison of the present predictions with previous works.

(a) Hedge-free case

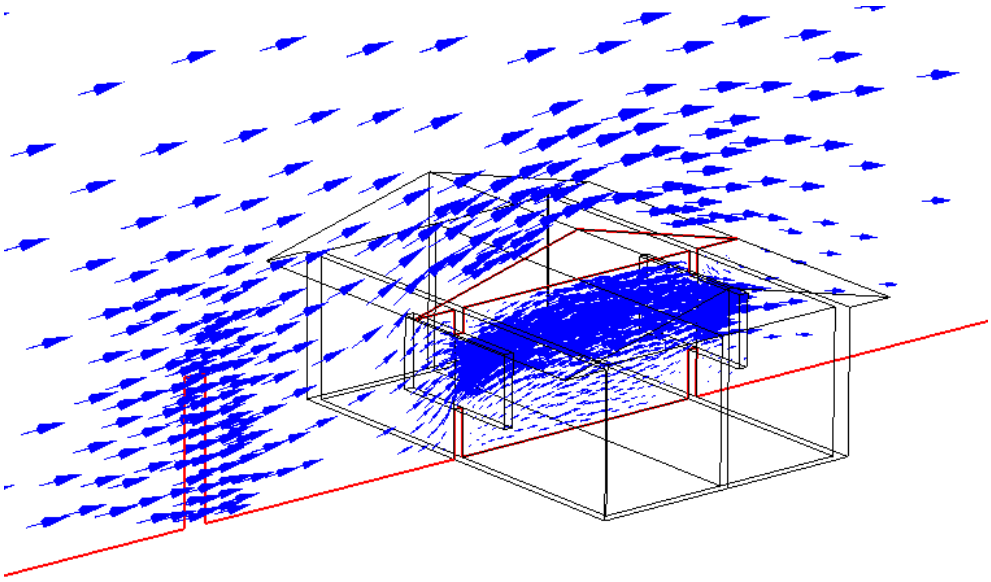

(b) Solid-hedge case (η=0)

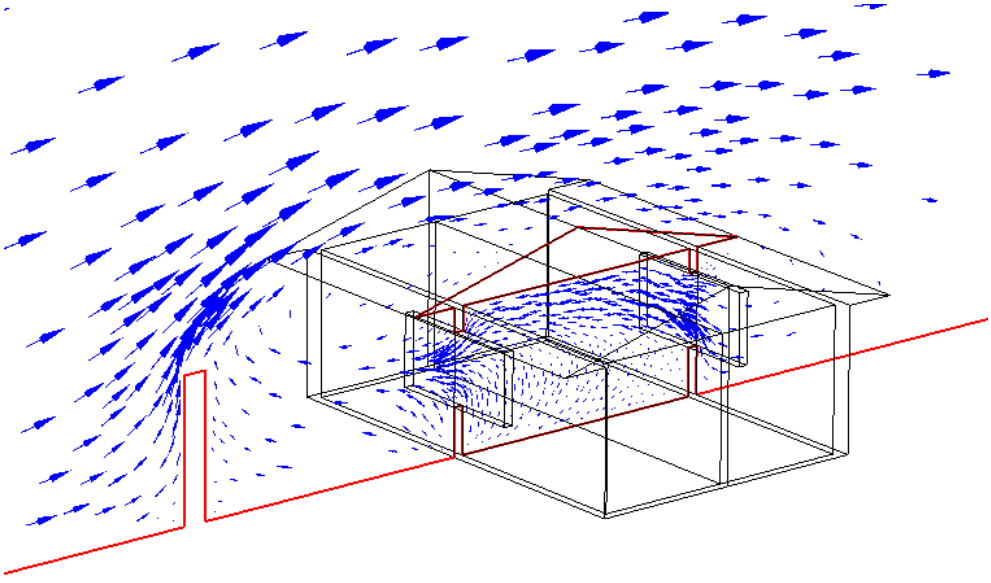

Figure 4 Comparison of mean-flow velocity vectors at the sectional plane cutting across the middle of the computational domain (y=0).

(a) Hedge-free case

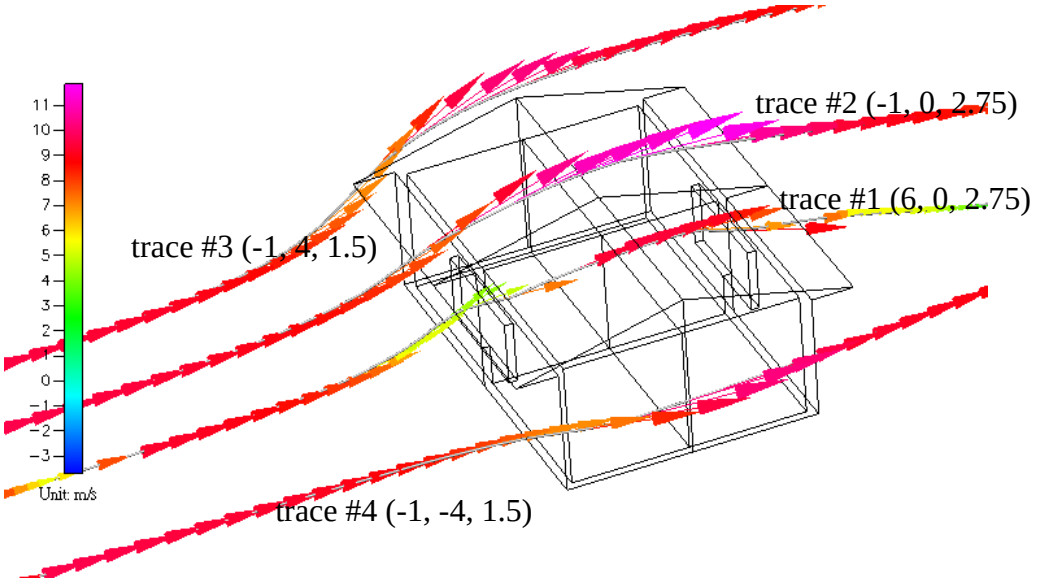

(b) Solid-hedge case

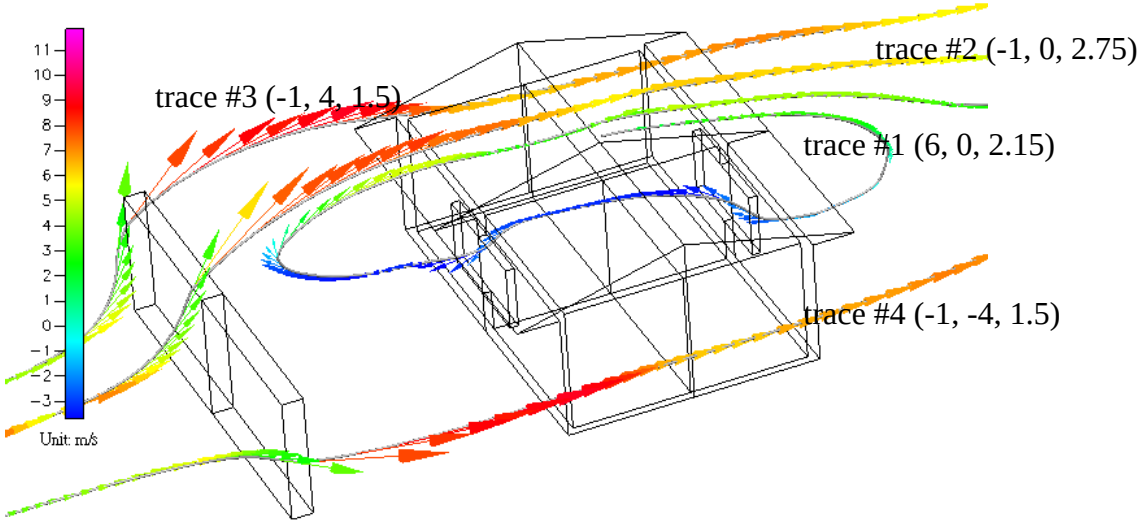

Figure 5 Particle traces around the building for the hedge-free and solid-hedge cases.

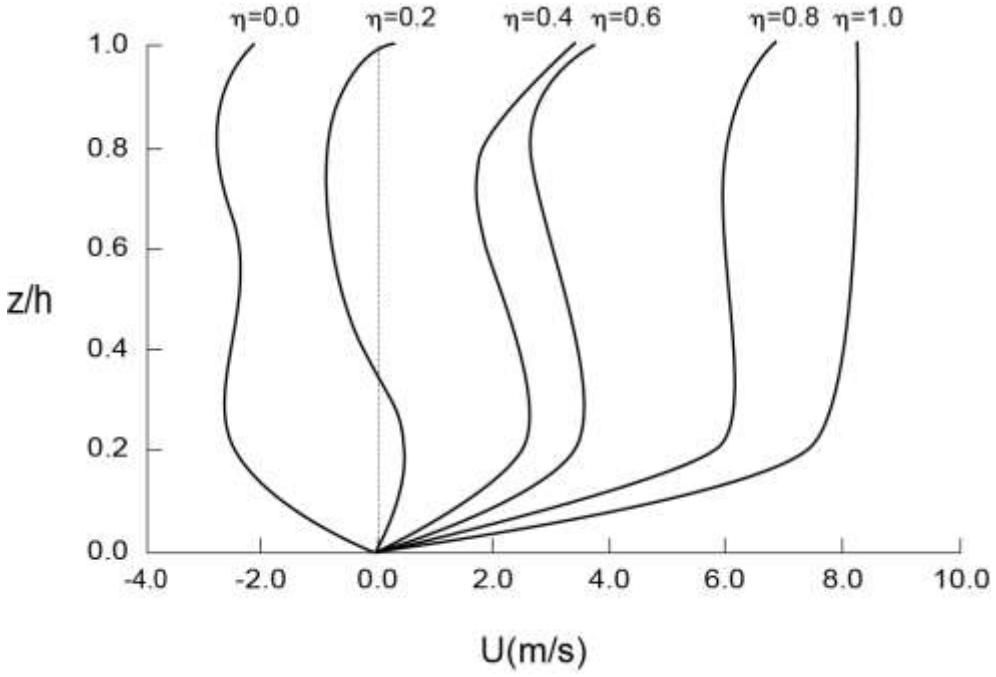

Figure 6 Axial mean velocity (*U*) distributions at the mid-station (*x*/h=1.0) between the porous hedge and the building on the module symmetric plane (*y*=0).

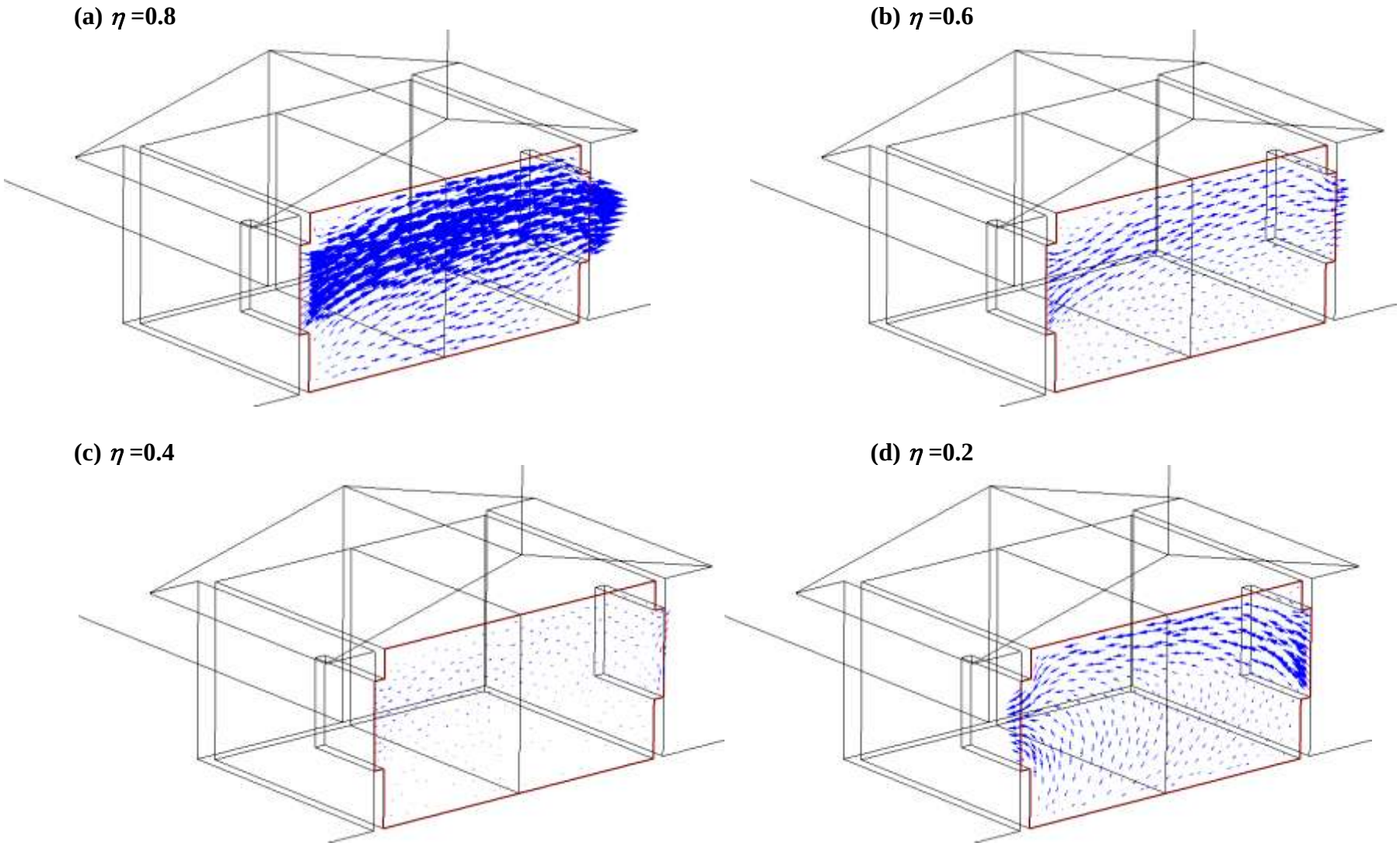

Figure 7 Effect of hedge porosity on the distributions of mean-flow velocities on the mid-plane (y=0) of the building.

(a) η **=0.8**

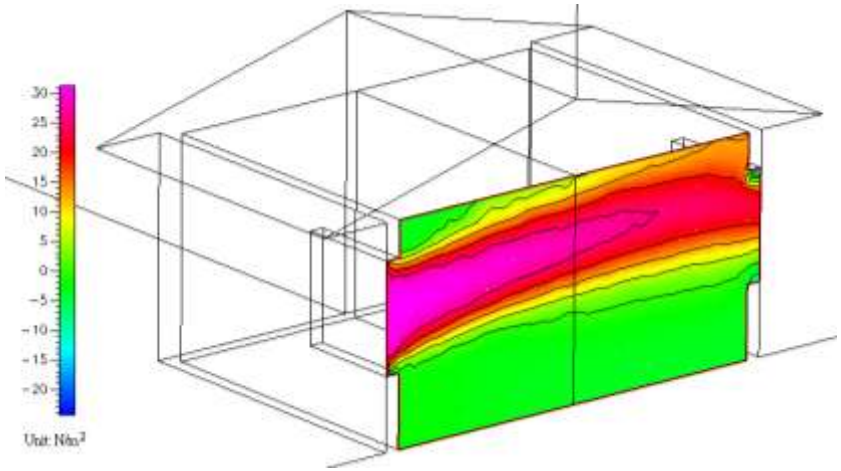

(b) η **=0.6**

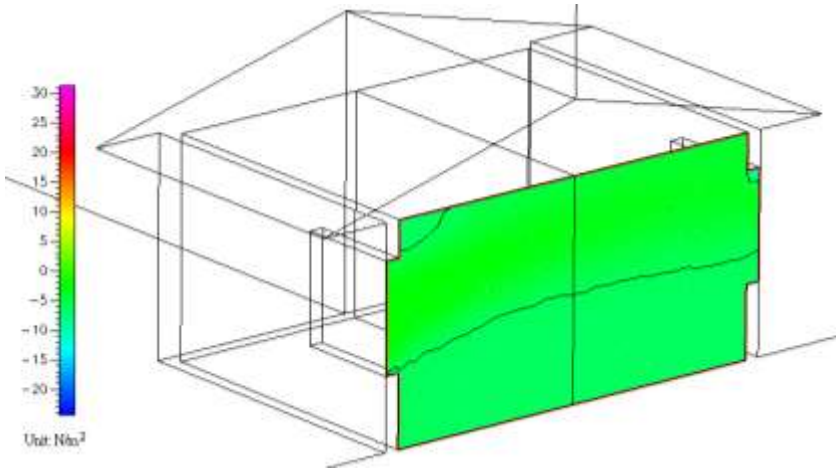

(c) η **=0.4**

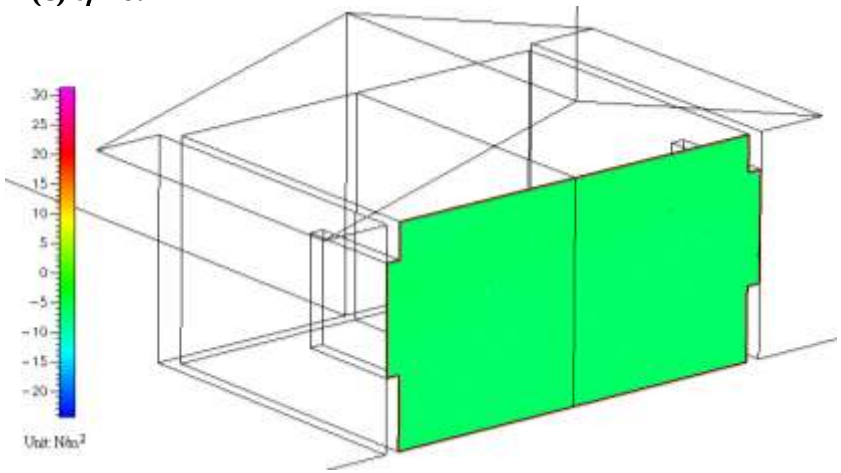

(d) η **=0.2**

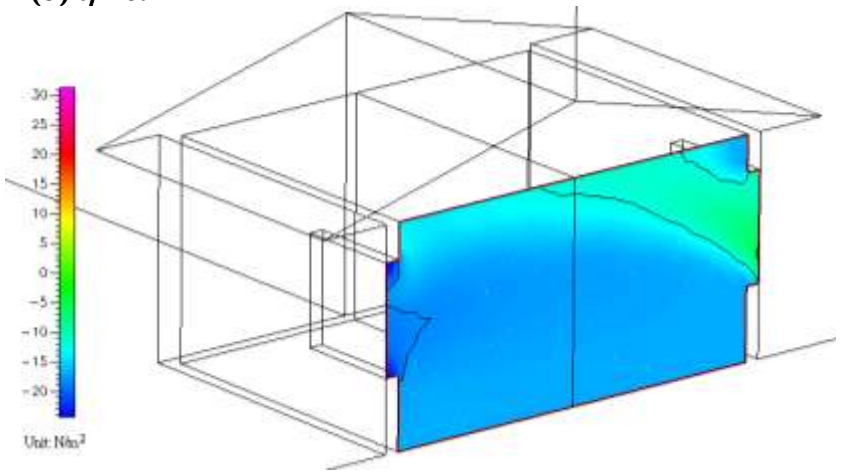

Figure 8 Effect of hedge porosity on the pressure distributions on the mid-plane (*y*=0) of the building.

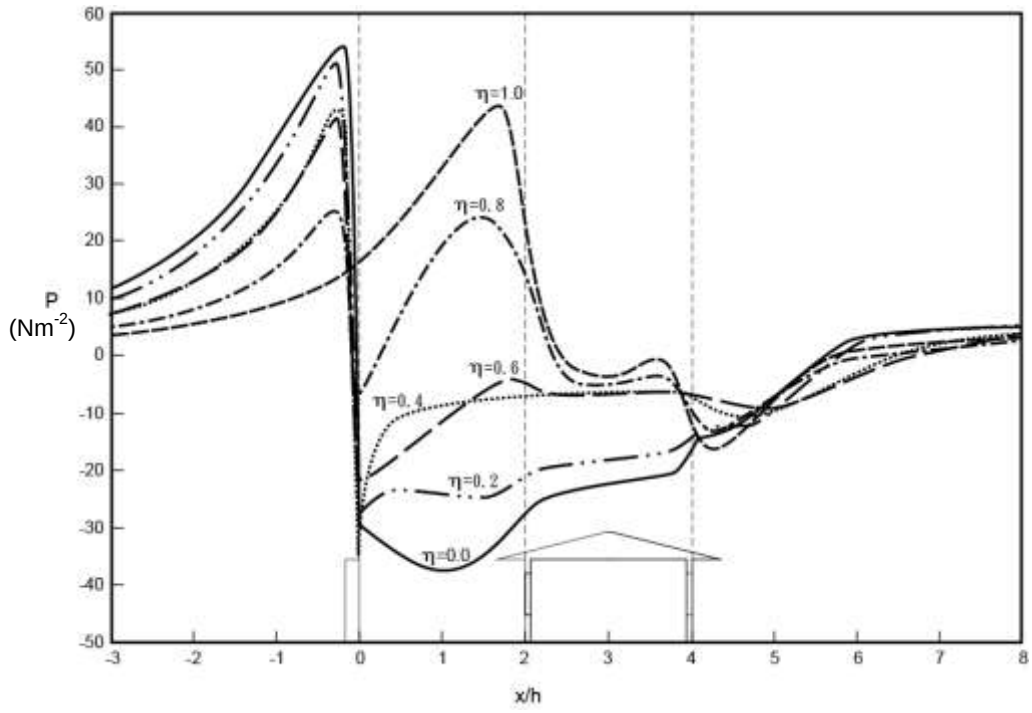

Figure 9 Pressure distributions at the elevation of *z*/h=0.58 along the flow direction on the symmetric plane (*y*=0) of the computational domain.

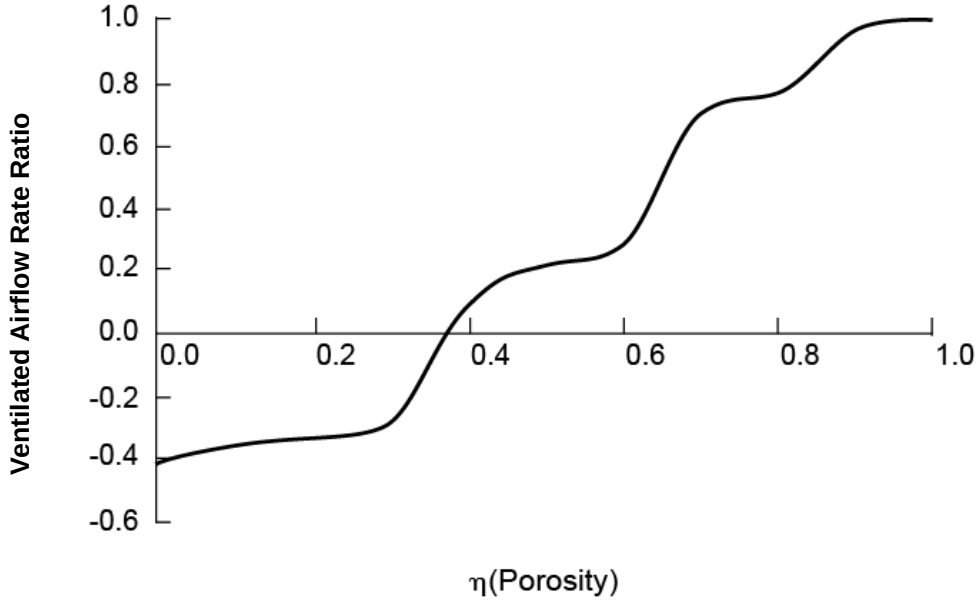

Figure 10 Effect of the hedge porosity on the ventilated airflow rate across the building.

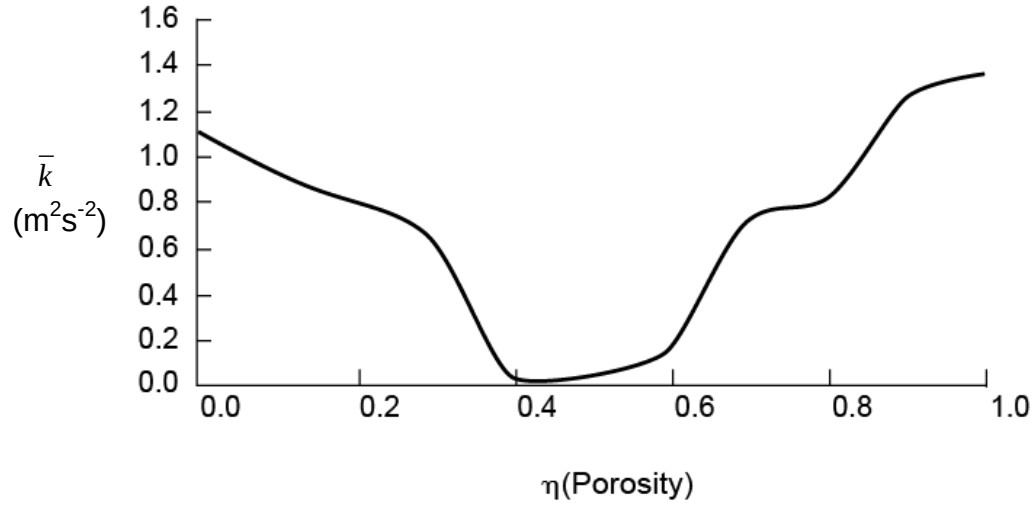

Figure 11 Effect of the hedge porosity on the volume-averaged turbulent kinetic energy in the building.

計畫成果自評:

本計畫完成之工作項目及成果

1. 完成工作項目

- 完成多孔植栽風擋計算流體力學三維模式之建立。
- 完成計算流體力學軟體之撰寫。
- 完成風擋非均一孔隙率對建築物室內外週圍氣流影響之分析與探討。
- 完成風擋相對長度對建築物室內外氣流影響之分析與探討。
- 完成建築物屋頂形式對建築物室內外氣流影響之分析與探討。
- 完成建築物開窗位置對建築物室內外氣流影響之分析與探討。
- 以風洞實驗（煙霧法）完成不同孔隙率風擋之流場可視化量測與分析。
- 以風洞實驗（煙霧法）完成不同長度風擋之流場可視化量測與分析。
- 完成不同孔隙率風擋流場壓力分佈之量測。
- 完成不同長度風擋流場壓力分佈之量測。
- 完成不同計算流體力學與風洞實驗結果之比較。
- 完成風擋之最佳化分析。

2. 完成成果

2.1 對於學術研究之貢獻

- 本計畫對植栽風擋影響建築物室內外氣流作有系統且完整之理論分析與實驗研究，對於國內景觀設計與自然通風之相關研究具有啟發作用，並積極取得與國際同步之研發水準。
- 本計畫成果已發表一篇研討會論文及一篇審查中期刊論文。
  - **W.R. Chang,** C.L. Cheng. (2007). Passive Control of Cross Ventilation in a Residential Building Using a Porous Hedge. *Building and Environment*. NSC 95-2415-H-216-002.[SCI]（in review）
  - **張瑋如**, “植栽風擋對住宅建築風力通風之影響—雙開窗模型之研究”,景觀論壇－永續景觀研討會, 新竹. 2006.12.

2.2 對國家發展及產業界之貢獻

- 本計畫所探討之風擋效應可作為內政部建築研究所「綠建築規劃設計技術彙編之研究」的進一步補充，有助於永續環境之設計。
- 本計畫之研發成果將可協助設計低耗能建築之設計、降低污染，促進國家之永續發展。
- 藉由本計畫進行與成果發表時，與國內外景觀與通風設計之研究學者進行互動合作。

2.3 參與之工作人員獲得之訓練

- 經由本計畫之執行，參與計畫之學生在研究執行過程中，獲得動手設計模型、操作儀器，以及分析實驗數據之能力。
- 參與工作人員已初步建立通風數學模式與撰寫程式之能力。